Synthetic Indices for Comfort Assessment: An Application to a Historical Building in Catania

Andrea Longhitano – University of Catania, Italy – andrea.longhitano@phd.unict.it
Gianpiero Evola – University of Catania, Italy – gevola@unict.it
Vincenzo Costanzo – University of Catania, Italy – vincenzo.costanzo@unict.it
Francesco Nocera – University of Catania, Italy – fnocera@unict.it

Abstract

This article presents a novel methodology that combines energy simulation and the use of advanced comfort indices for assessing thermal comfort in buildings, with a specific focus on a historical office building in Catania (Italy). The research methodology includes detailed modelling in TRNSYS, supported by surveys and on-site measurements of temperature and relative humidity. Then, suitable synthetic indices are introduced that are adaptable to different thermal comfort theories, in line with major standards (ASHRAE 55 and EN 16798-1, namely). This provides a versatile tool for assessing thermal discomfort in historical buildings while easily identifying the rooms where applying possible mitigation strategies is most urgent. This approach also allows us to evaluate the effect of suitable retrofitting options that could achieve good thermal comfort, thus reducing energy consumption and contributing to their adaptation to the evolving climate.

1. Introduction

The analysis of thermal comfort in the built environment is an increasingly prominent topic in engineering and architecture, driven by the need to enhance indoor environmental quality and to reduce the energy consumption in buildings.

The quantification of thermal comfort is critical: many studies have explored various indices, such as Predicted Mean Vote (PMV), Predicted Percentage of Dissatisfied (PPD) (Fanger, 1970), and Standard Effective Temperature (SET) (ANSI and ASHRAE, 2020; Silva et al., 2016; Tartarini and Schiavon, 2020) to assess comfort conditions in buildings. These indices, along with others like Intensity of Thermal Discomfort (ITD), Frequency of Thermal Comfort (FTC), Frequency of Thermal Discomfort (FTD), Fluctuation of thermal Discomfort (FD) (Detommaso et al., 2021; Evola et al., 2015; Sicurella et al., 2012), Passive Discomfort Index (Índice de Desconforto Passivo) (Dos Reis et al., 2022), ASHRAE Likelihood of Dissatisfaction and Nicol et al.'s Overheating Risk (Nicol et al., 2009), provide a solid foundation for optimizing building design and evaluating their operational thermal performance. In the context of historical buildings, these challenges are aggravated by architectural and conservation constraints, thus calling for innovative solutions to align thermal comfort with heritage preservation (Martínez-Molina et al., 2016).

This paper presents a novel approach for evaluating the thermal comfort in buildings over long time spans that integrates dynamic energy simulation with the application of advanced comfort indices to a case study building in Catania. The results also demonstrate that historical buildings, under current climatic conditions, may suffer from thermal discomfort issues, especially in the summer.

2. Material and Methods

2.1 Methodology

In this research, a comprehensive methodology was developed to facilitate the analysis of thermal comfort in historical buildings. The methodology is summarized in the flowchart of Figure 1.

Phase 1 requires detailed information to create a reliable virtual model, including the collection of geometric, morphological and thermophysical data.

Part of
Pernigotto, G., Ballarini, I., Patuzzi, F., Prada, A., Corrado, V., & Gasparella, A. (Eds.). 2025. Building simulation applications BSA 2024. bu,press.
https://doi.org/10.13124/9788860462022

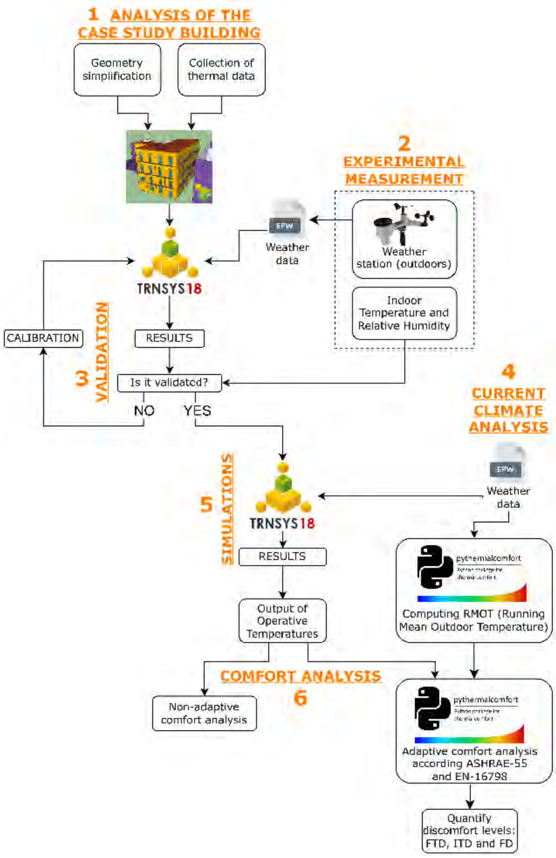

Fig. 1 – Workflow of the methodology

The process involves also simplifying the building's geometry and constructing a virtual model using the TRNSYS energy simulation software.

Phase 2 consists in carrying out preliminary experimental measurements, which is instrumental for the validation of the virtual model (phase 3). This step requires the collection of local meteorological data that is then used for a first run of simulations for validation purposes. Data regarding indoor air temperature and relative humidity are also collected to compare them with the simulation results. The validation is based on different error indices (Baggio et al., 2013), whose suggested thresholds (Huerto-Cardenas et al., 2020) are indicated in Table 1: MAE (Mean Absolute Error), RMSE (Root Mean Square Error), r (Pearson's Correlation Coefficient), R^2 (Coefficient of Determination).

Once the model is validated, simulations can be run with the current climate (phase 4), which is done by using the typical meteorological file of the city where the building is placed.

Table 1 – Suggested thresholds for error indices (Huerto-Cardenas et al., 2020)

	MAE	RMSE	r	R^2
LV 1	≤ 1 [°C – g/kg]	≤ 5 [%]	> 0.5	> 0.75
LV 2	≤ 2 [°C – g/kg]	≤ 10 [%]		

This step also includes the calculation of the Running Mean Outdoor Temperature (RMOT), which is necessary to compute the thermal comfort thresholds in line with the adaptive comfort theory (Humphreys et al., 2015; Yao et al., 2022). After the numerical simulations (phase 5), the outputs are then processed, with a focus on the operative temperature. The methodology requires two different analyses of thermal comfort (phase 6): a first one looks at the time trends of the indoor operative temperature, while the second one relies on the adaptive comfort approach in accordance with the American ASHRAE 55 (ANSI & ASHRAE, 2020) and the European EN 16798-1 (EN 16798-1:2019) standards. This second analysis requires the calculation of three discomfort indices: ITD [°C h], FTD [%] and FD [°C] (Evola et al., 2015; Sicurella et al., 2012), which refer only to those time intervals when the presence of the occupants is expected. More specifically, the ITD quantifies the degree hours by which room temperatures exceed the predefined thermal comfort thresholds:

$$ITD = \int_p \Delta T_{over}(\tau) \cdot d\tau \qquad \text{where}$$

$$\Delta T_{over}(\tau) = \begin{cases} T_{op}(\tau) - T_{over} & if \quad T_{op}(\tau) \geq T_{over} \\ 0 & if \quad T_{op}(\tau) < T_{over} \end{cases}$$

The subscript *over* refers to "*overheating*", i.e. thermal discomfort due to high indoor operative temperatures. The FTD measures the percentage of time within a given period when the indoor thermal comfort conditions are not met; it is determined by dividing the hours in which thermal discomfort is perceived by the total number of occupancy hours. Finally, the FD is the ratio of the ITD to the length of the period when thermal discomfort is perceived:

$$FD = \frac{ITD}{\int_p i_+ \cdot d\tau} \qquad \text{where}$$

$$i_+ = \begin{cases} 1 & if \quad T_{op}(\tau) \geq T_{over} \\ 0 & if \quad T_{op}(\tau) < T_{over} \end{cases}$$

In case of high ITD and low FD, the room is most probably often in the discomfort region, thus a general improvement in the thermal performance of the whole building fabric might be required. On the contrary, a high FD means that discomfort occurs rarely but in an intense way; in this case the problem could be tackled with a single local tailored solution, such as a higher ventilation rate or a more efficient shading device (Sicurella et al., 2012).

2.2 Case Study

The selected case study for this research is an office building belonging to the University of Catania, Italy, built in the first half of the 19th century and restored in the past decade. The building's masonry walls are made of volcanic stones and mortar. Wall thicknesses vary across different floors and for internal and external walls.

To create a reliable virtual model, detailed geometric, morphological, and thermophysical data were meticulously gathered. The model creation in TRNSYS meant simplifying the complex geometry, particularly the windows, which are arched but are modified to an equivalent rectangular shape while retaining the proportion of glazing to frame area.

Afterwards, the U-value of the external walls was measured, and an equivalent thermal conductivity was calculated to treat masonry walls as a uniform material. A detailed analysis of the occupancy rates per unit area in each floor provided also insights into utilization patterns. Validation of the virtual model was then undertaken by measuring indoor temperature and humidity in specific rooms during May and June 2023. Outdoor weather data from a local weather station were supplemented with solar radiation data from an online source, were used in the simulations (SIAS, 2023) (see Figure 2).

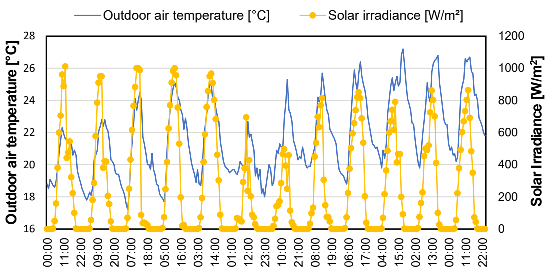

Fig. 2 – Outdoor air temperature and solar irradiance from May 31st to June 11th, 2023

After the construction and successful validation of the model (Huerto-Cardenas et al., 2020), a thermal comfort analysis was carried out. It aimed to identify the rooms with the greatest discomfort and the origins of such discomfort, with a particular focus on summer overheating during the months of June, July, August, and September.

Unlike the fixed comfort bands of non-adaptive theory, the adaptive comfort theory considers time-evolving comfort ranges that are based on outdoor conditions (Humphreys et al., 2015). An essential element in the calculation of adaptive comfort bands is the Running Mean Outdoor Temperature (RMOT), i.e. the mean outdoor temperature over a specified period (Yao et al., 2022). In this paper, RMOT has been calculated through the web tool developed by Tartarini and Schiavon (Tartarini & Schiavon, 2020). This tool allowed us to compute the adaptive comfort bands under different scenarios and considering two specific standards, the ASHRAE 55 and EN 16798-1 namely. ASHRAE 55 includes two performance categories, "80" and "90": "80" denotes comfort levels suitable for 80% of individuals while "90" indicates 90% of people satisfied (ANSI and ASHRAE, 2020). Instead, the EN 16798-1 defines three performance categories: "Category III," "Category II," and "Category I". "Category III" represents lower comfort levels, accepted by a smaller percentage of occupants; "Category I" concerns the highest comfort performance, while "Category II" stands as an intermediate category (EN 16798-1:2019). After calculating the adaptive comfort bands, the operative temperatures of the room were evaluated, examining whether they fell within or exceeded these comfort thresholds. Further analyses quantified discomfort in the thermal zones by using the Intensity of Thermal Discomfort (ITD), Frequency of Thermal Discomfort (FTD), and Fluctuation of thermal Discomfort (FD), specifically during occupancy hours (8 AM to 6 PM).

2.3 Simplification and Modelling of the Case Study Building

The modelling was carried out within the TRNSYS energy simulation software tool (Figure 3 shows an axonometric view of the real virtual building).

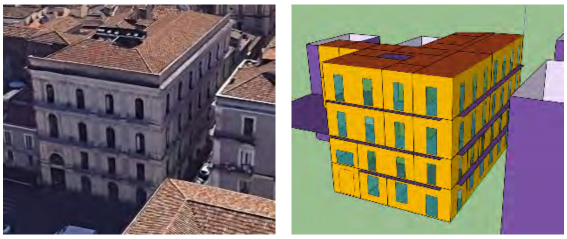

Fig. 3 – Case study building and model

To accurately capture the intricacies of the historical building's thermal behaviour, several considerations and simplifications were made. Notably, the thermal zones within the building were defined by merging the rooms sharing common attributes, such as orientation (North, South, East, or West) and function, resulting in 41 thermal zones (the actual number of rooms is 70 instead).

Coherently, internal partitions between rooms pertaining to the same thermal zone were omitted from the geometric model. These thermal zones were, however, manually assigned augmented thermal capacity to compensate for the absence of the massive internal walls. To quantify the thermal capacity of the omitted walls, the computation of volumes of walls included in each thermal zone was carried out, while the specific heat capacity (c_p) is set to 1 $kJ \cdot kg^{-1} \cdot K^{-1}$ and the density (ρ) is 2400 $kg \cdot m^{-3}$ (Gagliano et al., 2014; UNI 10351:2021; UNI 10355:1994). Wall thicknesses vary across different floors and across internal and external walls. The following measurements were adopted: for external walls facing the street, the masonry thicknesses are 120 cm (ground floor), 105 cm (first floor), 90 cm (second floor), and 75 cm (third floor). In contrast, for external walls facing the courtyard the masonry thicknesses are 90 cm (ground floor), 80 cm (first floor), 70 cm (second floor), and 60 cm (third floor). For internal walls separating individual rooms the thicknesses are 80 cm (ground floor), 65 cm (first floor), 45 cm (second floor), and 30 cm (third floor).

Additionally, architectural features such as light wells on the second and third floors were represented as void spaces. A shading surface was introduced above these light wells, emulating the grilled structure where the thermal systems are placed. Distinct net height measurements were attributed to each floor, because on some floors there are counter ceilings and on other vaults: 5.30 m for the ground floor, 4.70 m for the first floor, and 5.70 m for both the second and third floors. Many rooms featured vaulted ceilings and non-rectangular doors and windows: these complexities were simplified by approximating rooms as rectangular boxes, but ensuring the same floor surface area and room volume (Elhadad et al., 2020). The same applies to doors and windows, where the simplifications did not affect the glazing and frame surfaces. The building has different types of windows, in terms of frame materials, geometric shape and ratio of opaque and transparent surfaces. Primarily, some windows have wooden frames, with a thickness of 6 cm and a thermal transmittance U = 1.67 $W \cdot m^{-2} \cdot K^{-1}$, whereas others have metal frames without a thermal break, with a thickness of 7 cm and U = 5.85 $W \cdot m^{-2} \cdot K^{-1}$. The type of glass employed is consistent across all window types, comprising laminated glass with 8 mm thickness. This glass has thermal transmittance U_g = 5.6 $W \cdot m^{-2} \cdot K^{-1}$, and g = 0.89 (solar heat gain coefficient). As previously written, the diversity of window types encompasses variances in geometric shape and size (Figure 4), leading to a simplification process: Table 2 describes in detail the areas of transparent and opaque surfaces for each type. Furthermore, balconies were simplified: they were merged into a single longer surface. Surrounding buildings were incorporated as shading elements (see Figure 3).

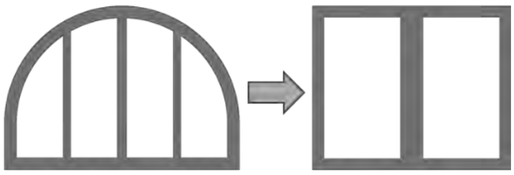

Fig. 4 – Simplification of windows geometry (Type D)

Table 2 – Transparent and opaque surface areas for windows

Type	Transparent surface area	Opaque surface area	Type	Transparent surface area	Opaque surface area
	[m²]	[m²]		[m²]	[m²]
A	4.17	2.41	I	0.56	0.25
B	4.92	1.20	J	6.46	1.83
C	3.64	2.48	K	1.53	1.41
D	4.05	1.97	L	3.30	3.74
E	2.76	1.72	M	1.72	1.14
F	3.36	2.70	N	2.12	2.05
G	2.89	4.08	O	4.64	0.29
H	2.03	2.13			

The attic space was not included in the model, so the last floor ceiling surfaces were assigned specific boundary conditions for heat exchange with the underlying zones. Subsequently, settings for infiltration were established, specifying an infiltration rate of 0.30 air changes per hour (UNI/TS 11300:2014). The number of luminaires, each hosting two 55 W halogen lamps, is reported in Table 3 for each thermal zone: the lighting schedule is aligned with standard office hours, activated from 7:00 AM to 6:00 PM. Electrical equipment generates 5 W·m^{-2} heat gains.

Table 3 – Number of light points for each thermal zone

T. Zone	Light points	T. Zone	Light points	T. Zone	Light points	T. Zone	Light points
001	4	**101**	4	**201**	8	**301**	8
002	7	**102**	4	**202**	4	**302**	4
003	23	**103**	4	**203**	12	**303**	12
004	2	**104**	20	**204**	16	**304**	16
005	2	**105**	10	**205**	10	**305**	10
006	10	**106**	4	**206**	2	**306**	2
007	6	**107**	2	**207**	11	**307**	8
008	10	**108**	6	**208**	4	**308**	4
		109	10	**209**	2	**309**	2
		110	2	**210**	2	**310**	2
		111	4	**211**	3	**311**	3

2.3.1 Experimental Measurement for modelling and validation purpose

An experimental campaign to measure the U-value of external walls was conducted between 6th and 13th March 2023 by using a Thermozig heat flow meter, whose technical features are listed in Table 4.
The U-value measurements specifically targeted the walls of selected rooms that were unoccupied due to staff absence. In adherence to (ISO 9869:2014), the selected walls were north-facing, and space heating was turned on during the campaign to increase the indoor-outdoor temperature drop. The duration of the measurements amounted to 167 hours. The results of these measurements revealed that the U-value of the external walls was around 1.15 W·m^{-2}·K^{-1}. Since the wall thickness is 0.70 m, this corresponds to an equivalent thermal conductivity λ_{eq} = 1 W·m^{-1}·K^{-1}. Between May 31st and June 11th, 2023, another monitoring campaign was performed in two unoccupied thermal zones, denoted as 203 and 303, located respectively at the second and third floor.

Table 4 – Technical features of Thermozig heat flow meter

	Temperature	Heat Flow
Measuring Range	from -50°C to 125°C	from -300 to 300 W·m^{-2} *(from -20°C to 60°C)*
Resolution	0.01°C	0.01 W·m^{-2}
Accuracy	± (0.10+0.0017∣t∣) °C	± 5% (@T = 20°C)

More specifically, two Wöhler CDL 210 dataloggers (technical features are listed in Table 5) were used for measuring air Temperature and Relative Humidity that were then used to validate the virtual model. A graph of the temperature and relative humidity achieved in the measurement campaign is included in Figure 5.

Table 5 – Technical features of Wöhler CDL 210 datalogger

	Temperature	Relative Humidity
Measuring Range	from -10°C to 60°C	5% to 95%
Resolution	0.1°C	0.1%
Accuracy	± 0.6°C	± 3% for 10% and 90% ± 5% otherwise

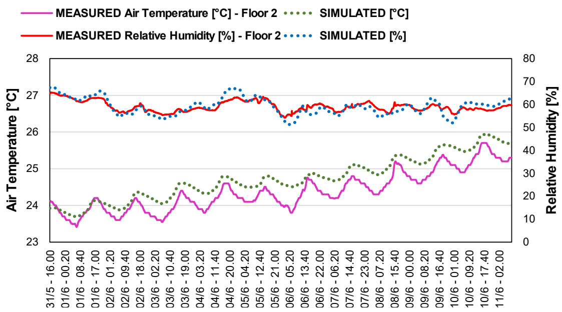

Fig. 5 – Temperature and relative humidity values (from May 31st to June 11th, 2023) (Thermal Zone 203)

2.3.2 Occupancy profiles of rooms

In the simulations, sedentary office workers were considered, with a thermal power of approximately 115 W per person (Sansaniwal et al., 2022). To calculate the total heating load for each thermal zone, this per-person power value was multiplied by the number of workstations and by the actual occupancy rate of workstations (Figure 6). Due to privacy and the lack of more granular data, these calculations were detailed at the floor level rather than at the room level. There are 17 workstations on the ground floor, 31 on the first floor, 34 on the second floor, and 28 on the third floor.

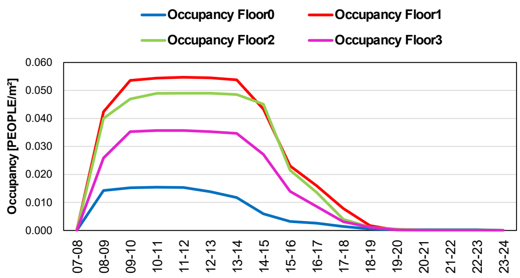

Fig. 6 – Workstations' occupancy rate for each floor

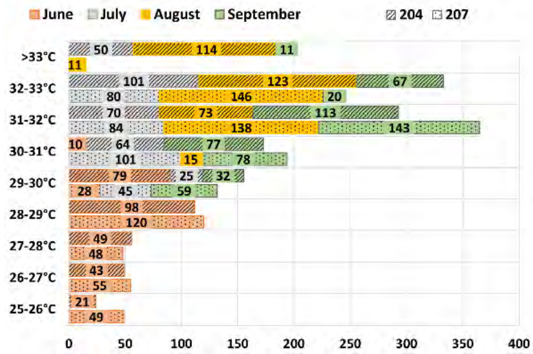

Fig. 7 – Operative temperature distribution (Zone 204 and 207)

3. Results and Discussion

3.1 Validation of the Virtual Model

As a result of this simulation, air temperature and relative humidity values were obtained and are shown in Figure 5. Moreover, Table 6 and Table 7 show the error index regarding the validation. The error index values were compared with the values suggested by (Huerto-Cardenas et al., 2020) and, as they fall within acceptable ranges, the model shows good agreement with real-world measurements.

Table 6 – Temperature error indices

Thermal Zone	MBE	MAE	RMSE	r	R^2
	[°C]	[°C]	[°C]		
203	-0.35	0.35	0.38	0.96	0.93
303	-0.14	0.26	0.31	0.92	0.85

Table 7 – Relative humidity error indices

Thermal Zone	MBE	MAE	RMSE	r	R^2
	[%]	[%]	[%]		
203	0.03	1.74	2.11	0.85	0.78
303	2.12	2.38	2.83	0.84	0.76

3.2 Comfort Analysis

By using the validated model, a set of free-floating dynamic simulations was conducted. First, the frequency distribution of the operative temperature was analysed in each thermal zone: Figure 7 reports the results in Zone 204 (second floor, facing West) and Zone 207 (facing East towards the internal courtyard) in June, July, August, and September. These zones show high levels of discomfort: in Zone 204 the most frequent operative temperature range is 31 °C and 33 °C, with a total of almost 550 hours; in Zone 207 the most frequent range is also between 31 °C and 33 °C with a total of over 600 hours, but here we also observe 175 hours above 33 °C.

Based on these results only, identifying the thermal zones with the most severe thermal condition is not straightforward, even because the building has 70 rooms divided into 41 thermal zones. This is precisely the point where the utility of the ITD becomes evident: indeed, with a single number it provides a clear indication of both intensity and duration of thermal discomfort.

In this case, the ITD, FTD and FD were computed for each thermal zone against the adaptive comfort bands, whereby the comfort thresholds are not constant with time. In principle, all possible performance categories were considered ("90" and "80" in ASHRAE 55 plus "Category I", "Category II" and "Category III" in EN 16798-1). However, since this is an office building it is reasonable to refer mostly to "Category II" in the EN 16798-1 Standard and "80" in the ASHRAE 55 Standard.

Figure 8 shows the ITD values across all thermal zones, reflecting also the variations within performance categories. These results confirm that the ITD is a valid synthetic index and they emphasize that – even when employing the more flexible adaptive comfort approach – several thermal zones may still experience thermal discomfort due to overheating in the absence of cooling systems. For instance, the ITD values in Zone 204 (ITD = 2387) and Zone 207 (ITD = 1876) are high, if compared e.g. with Zone 206 (ITD = 653) and Zone 211 (ITD = 441). There is currently no official reference to a maximum allowed ITD value, but in comparative terms this index immediately identifies the critical rooms where measures are urgently needed to improve thermal comfort. For instance, the rooms on the third floor are on average far less comfortable than on the ground floor.

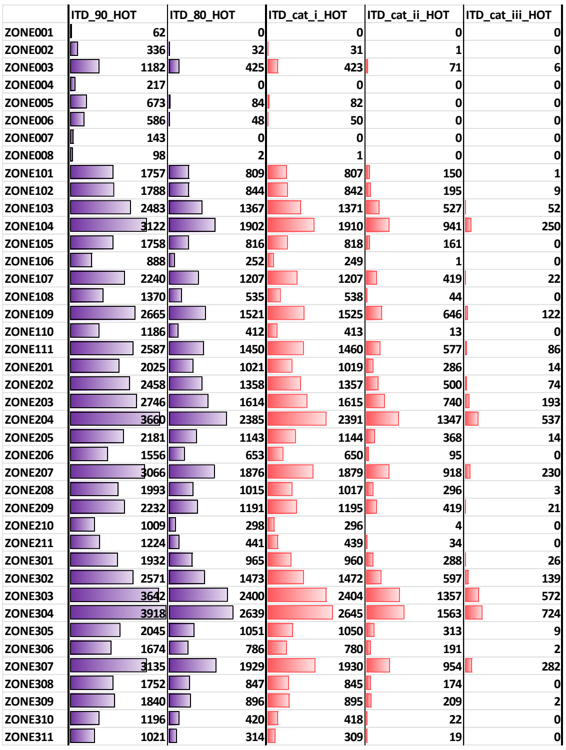

Fig. 8 – Intensity of Thermal Discomfort in the 41 thermal zones (purple: ASHRAE 55 - red: EN 16798-1)

Table 8 – Frequency of Thermal Discomfort (Zones 204 and 207)

	FTD - "Category II" EN 16798-1		FTD - Category "80" ASHRAE 55	
	Thermal Zone 204	**Thermal Zone 207**	**Thermal Zone 204**	**Thermal Zone 207**
June	11%	4%	55%	30%
July	98%	92%	100%	100%
August	100%	100%	100%	100%
September	99%	100%	100%	100%

Table 9 – Fluctuation of thermal Discomfort (Zones 204 and 207)

	FD - "Category II" EN 16798-1		FD - Category "80" ASHRAE 55	
	Thermal Zone 204	**Thermal Zone 207**	**Thermal Zone 204**	**Thermal Zone 207**
June	0.5	0.1	0.6	0.4
July	1.6	1.1	2.6	2.0
August	2.3	1.5	3.3	2.5
September	1.4	1.1	2.4	2.1

Of course, ITD = 0 indicates that a room does not show any overheating issue (Zone 007). Still focusing on Zone 204 and Zone 207, Table 8 and Table 9 report the FTD and FD values, according to "Category II" of EN 16798-1 and Category "80" of ASHRAE 55. The FTD values in Table 8 show that discomfort conditions occur very frequently in both zones, especially in light of the ASHRAE 55 Standard, which is more stringent than "Category II" of EN 16798-1. The FD values are low (Table 9), which suggests steady thermal discomfort.

4. Conclusion

This research developed a simulation framework in TRNSYS to build up and validate a multi-zone model for complex historical buildings with the aim of appraising thermal discomfort in summer. A series of suitable modelling simplifications in terms of geometry and thermal features are introduced in order to keep a reasonable level of detail while reducing the burden of the modelling task. Then, synthetic thermal comfort indices such as the Intensity of Thermal Discomfort (ITD) and the Frequency of Thermal Discomfort (FTD) are applied based on the adaptive comfort theory, to quickly identify the thermal zones that suffer the most from thermal discomfort. The application to a case study in Catania (Southern Italy) proved very effective to easily identify those rooms that urgently call for passive solutions to mitigate indoor overheating, while also informing if discomfort is frequent and steady. The methodology can be extended to other multi-zone buildings even other than offices. Future research is planned to include also the effect of climate change in the simulation framework, by suitably modifying the weather data input.

Nomenclature

c_p	Specific heat capacity ($J \cdot kg^{-1} \cdot K^{-1}$)
FD	Fluctuation of thermal Discomfort
FTD	Frequency of Thermal Discomfort
ITD	Intensity of Thermal Discomfort
MAE	Mean Absolute Error
PMV	Predicted Mean Vote
PPD	Predicted Percentage of Dissatisfied
r	Pearson's Correlation Coefficient
RMSE	Root Mean Square Error
RMOT	Running Mean Outdoor Temperature (°C)
R^2	Coefficient of Determination
T	Temperature (°C)
U	Thermal transmittance ($W \cdot m^{-2} \cdot K^{-1}$)
λ	Thermal conductivity ($W \cdot m^{-1} \cdot K^{-1}$)
ρ	Density ($kg \cdot m^{-3}$)

References

ANSI, and ASHRAE. (2020). *Standard 55 - Thermal Environmental Conditions for Human Occupancy*.

Baggio, P., Pernetti, R., and Prada, A. (2013). *Simulazione energetica degli edifici esistenti. Guida alla definizione di modelli calibrati* (EPC Editore, Ed.).

Detommaso, M., Gagliano, A., Marletta, L., and Nocera, F. 2021. "Sustainable urban greening and cooling strategies for thermal comfort at pedestrian level". *Sustainability*, *13*(6), 3138. https://doi.org/10.3390/su13063138.

Dos Reis, A. S., Vaquero, P., Dias, M. F., and Tavares, A. 2022. "Passive Discomfort Index as an alternative to Predicted Mean Vote and Predicted Percentage of Dissatisfied to assess occupant's thermal discomfort in dwellings". *Energy Reports*, *8*, 956–965. https://doi.org/10.1016/j.egyr.2022.07.128

Elhadad S., Radha C., Kistelegdi I., Baranyai B., and Gyergyák J. 2020. "Model Simplification on Energy and Comfort Simulation Analysis for Residential Building Design in Hot and Arid Climate". *Energies*, 13(8), 1876. https://doi.org/10.3390/en13081876

EN 16798-1: 2019 Energy Performance of Buildings—Ventilation for Buildings—Part 1: Indoor Environmental Input Parameters for Design and Assessment of Energy Performance of Buildings Addressing Indoor Air Quality (2019).

Evola, G., Marletta, L., Costanzo, V., and Caruso, G. 2015. "Different Strategies for Improving Summer Thermal Comfort in Heavyweight Traditional Buildings". *Energy Procedia*, *78*, 3228–3233. https://doi.org/10.1016/j.egypro.2015.11.785

Fanger, P. O. (1970). Thermal comfort. *Thermal Comfort. Analysis and Applications in Environmental Engineering*.

Gagliano, A., Patania, F., Nocera, F., and Galesi, A. 2014. "Performance assessment of a solar assisted desiccant cooling system". *Thermal Science*, *18*(2), 563–576. https://doi.org/10.2298/TSCI120526067G

Huerto-Cardenas, H. E., Leonforte, F., Aste, N., Del Pero, C., Evola, G., Costanzo, V., and Lucchi, E. 2020". Validation of dynamic hygrothermal simulation models for historical buildings: State of the art, research challenges and recommendations". *Building and Environment*, *180*, 107081. https://doi.org/10.1016/j.buildenv.2020.107081

Humphreys, M., Nicol, F., and Roaf, S. (2015). *Adaptive Thermal Comfort: Foundations and Analysis*. Routledge. https://doi.org/10.4324/9781315765815.

ISO 9869:2014 Thermal insulation - Building elements - In-situ measurement of thermal resistance and thermal transmittance - Part 1: Heat flow meter method. (2014).

Martínez-Molina, A., Tort-Ausina, I., Cho, S., and Vivancos, J.-L. 2016. "Energy efficiency and thermal comfort in historic buildings: A review". *Renewable and Sustainable Energy Reviews*, *61*, 70–85. https://doi.org/10.1016/j.rser.2016.03.018

Nicol, J. F., Hacker, J., Spires, B., and Davies, H. 2009. "Suggestion for new approach to overheating diagnostics". *Building Research & Information*, *37*(4), 348–357.

Sansaniwal S., Mathur J., and Mathur S. 2022. "Review of practices for human thermal comfort in buildings: present and future perspectives". *International Journal of Ambient Energy*, 43(1), 2097-2123. https://doi.org/10.1080/01430750.2020.1725629

SIAS. (2023). *Sistema Informativo Agrometeorologico Siciliano*. http://www.sias.regione.sicilia.it/

Sicurella, F., Evola, G., and Wurtz, E. 2012. "A statistical approach for the evaluation of thermal and visual comfort in free-running buildings". *Energy and Buildings*, *47*, 402–410. https://doi.org/10.1016/j.enbuild.2011.12.013

Silva, A. S., Ghisi, E., and Lamberts, R. 2016. "Performance evaluation of long-term thermal comfort indices in building simulation according to ASHRAE Standard 55". *Building and Environment*, *102*, 95–115. https://doi.org/10.1016/j.buildenv.2016.03.004

Tartarini, F., and Schiavon, S. 2020. "Pythermalcomfort: a Python package for thermal comfort research". *SoftwareX*, *12*, 100578. https://doi.org/10.1016/j.softx.2020.100578

UNI 10351:2021. Materiali da costruzione - Proprietà termoigrometriche - Procedura per la scelta dei valori di progetto (2021).

UNI 10355:1994. Murature e solai. Valori della resistenza termica e metodo di calcolo (1994).

UNI/TS 11300:2014. Prestazioni energetiche degli edifici (2014).

Yao, R., Zhang, S., Du, C., Schweiker, M., Hodder, S., Olesen, B. W., Toftum, J., Romana d'Ambrosio, F., Gebhardt, H., Zhou, S., Yuan, F., and Li, B. 2022". Evolution and performance analysis of adaptive thermal comfort models – A comprehensive literature review". *Building and Environment, 217*, 109020. https://doi.org/10.1016/j.buildenv.2022.109020.